fractal and fractional

MDPI

Article

Pore Structural and Fractal Analysis of the Effects of MgO Reactivity and Dosage on Permeability and F–T Resistance of Concrete

Lei Wang [1,2,*], Xuefeng Song [2,*], Huamei Yang [1], Lei Wang [1], Shengwen Tang [3], Bo Wu [1] and Wenting Mao [4]

[1] School of Intelligent Construction, Wuchang University of Technology, Wuhan 430002, China; yanghuamei@wust.edu.cn (H.Y.); 120100549@wut.edu.cn (L.W.); 120130069@wut.edu.cn (B.W.)
[2] College of Materials Science and Engineering, Xi'an University of Architecture and Technology, Xi'an 710055, China
[3] State Key Laboratory of Water Resources and Hydropower Engineering Science, Wuhan University, Wuhan 430002, China; tangsw@whu.edu.cn
[4] Yunnan Academy of Building Research, Kunming 650223, China; wm280@alumni.cam.ac.uk
* Correspondence: wanglei535250684@xauat.edu.cn (L.W.); songxuefeng@xauat.edu.cn (X.S.)

Abstract: Currently, the MgO expansion agent is widely used to reduce the cracking risk of concrete. The influence of MgO reactivity (50 s and 300 s) and dosage (0, 4 wt.% and 8 wt.%, by weight of binder) on the air void, pore structure, permeability and freezing–thawing (F–T) resistance of concrete were studied. The results indicate (1) the addition of 4–8 wt.% reactive MgO (with reactivity of 50 s and termed as M50 thereafter) and weak reactive MgO (with reactivity of 300 s and termed M300 thereafter) lowers the concrete's compressive strength by 4.4–17.2%, 3.9–16.4% and 1.9–14.6% at 3, 28 and 180 days, respectively. The increase in MgO dosage and reactivity tends to further reduce the concrete strength at all hydration ages. (2) Permeability of the concrete is closely related to the pore structure. M50 can densify the pore structure and lower the fraction of large capillary pores at an early age, thus it is beneficial for the impermeability of concrete. In contrast, M300 can enhance the 180-day impermeability of concrete since it can densify the pore structure only at a late age. (3) The influence of MgO on F–T resistance is minor since MgO could not change the air void parameters. (5) MgO concretes exhibit obvious fractal characteristics. The fractal dimension of the pore surface (D_s) exhibits a close relationship with the permeability property of concrete. However, no correlation can be found between F–T resistance and D_s.

Keywords: MgO; permeability; F–T resistance; pore; air void; fractal dimension

check for updates

Citation: Wang, L.; Song, X.; Yang, H.; Wang, L.; Tang, S.; Wu, B.; Mao, W. Pore Structural and Fractal Analysis of the Effects of MgO Reactivity and Dosage on Permeability and F–T Resistance of Concrete. *Fractal Fract.* **2022**, *6*, 113. https://doi.org/10.3390/fractalfract6020113

Academic Editors: Zine El Abiddine Fellah and Wojciech Sumelka

Received: 20 January 2022
Accepted: 12 February 2022
Published: 15 February 2022

Publisher's Note: MDPI stays neutral with regard to jurisdictional claims in published maps and institutional affiliations.

Copyright: © 2022 by the authors. Licensee MDPI, Basel, Switzerland. This article is an open access article distributed under the terms and conditions of the Creative Commons Attribution (CC BY) license (https://creativecommons.org/licenses/by/4.0/).

1. Introduction

With the rapid construction of infrastructure, the cracking of concrete structures has become a global concern in the field of civil engineering [1–6]. During the past decades, researchers have proposed many measures to reduce the cracking risk of concrete, including the usage of a certain amount of fly ash [7,8], shrinkage–reducing admixtures (SRA) [9], fibers [10–15] and magnesia expansion agent (abbreviated as MgO thereafter) [16,17], etc. Since the 1970s, MgO has been increasingly used in various concrete structures. The reaction between MgO and water produces $Mg(OH)_2$ crystals [18], the growth of which could generate expansion and compensate for the shrinkage of concrete [1].

MgO is typically produced by calcining magnesite at high temperatures. Its reactivity is dominated by the calcination conditions, e.g., calcination temperature and calcination time [1]. The reactivity and dosage of MgO are the two main factors affecting the expansion properties of concrete [19]. So far, there have been many studies concerning the effects of MgO reactivity and dosage on the shrinkage behavior, strength and microstructure of concrete as well as the cement hydration [16,18–23]. For instance, the reactive MgO reacts with water rapidly and produces a large expansion at an early age, therefore it was

suitable for compensating the early rapid shrinkage of thin concrete structures [16,20–22]. In contrast, weak reactive MgO reacts with water more slowly and produces a slower expansion at an early age but produces a larger expansion at a later age than the reactive one, thus it is more beneficial in compensating for the shrinkage of massive concrete structures at a later hydration age [16,20,22]. Generally, the shrinkage compensation effect of MgO enhances with the increase in MgO dosage [18,19]. In addition to shrinkage and strength, concrete durability is closely related to the safety and service life of concrete structures. Nevertheless, the studies regarding the influence of MgO on the durability of concrete are relatively limited. Commonly, permeability and freezing–thawing (F–T) resistance are two important parameters evaluating the durability of concrete.

There are some studies regarding the effects of MgO on the permeability property of concrete. Zheng et al. [24] indicated that the presence of MgO could modify the pore structures of concrete and consequently affect the permeability properties since the permeability of concrete was governed by the volume fraction (total porosity) and microgeometry of the entire pore structure. Choi et al. [25] reported that the addition of 5 wt.% MgO with a weak reactivity of about 210–265 s improved the resistance of fly ash concrete to chloride permeability in the long term by reducing the total porosity of concrete, especially by reducing the proportion of 0.03–0.3 μm pores. Jiang et al. [26] found that MgO with a 115 s reactivity enhanced the resistance to chloride penetration of bridge deck concrete, which is also closely related to the reduced porosity and optimized pore structure of concrete. A similar finding was reported by Sherir et al. [27] who found the addition of 5 wt.% MgO (without the reactivity information) improved the long-term chloride resistance of a self-healed cementitious composite. Nevertheless, to the best of our knowledge, no report exists to date describing the influence of the reactivity and dosage of MgO on the permeability of concrete.

The effects of MgO on the freezing–thawing (F–T) resistance of concrete have also been studied by researchers. Choi et al. [25] revealed that the addition of 5 wt.% (by weight of the binder) of a MgO expansive agent with reactivity of 210–265 s had little effect on the F–T resistance of concrete, since the MgO of this reactivity did not change the fraction of the pores larger than 10 μm (also termed the air void), which were often associated with F–T resistance. Gao et al. [17] found that the strength and mass losses of roller-compacted concrete (RCC) during the F–T cycles decreased with the increase in MgO dosage from 0 to 12 wt.%; that is, the F–T resistance of concrete is significantly enhanced with MgO dosage. It is well demonstrated that the F–T resistance of concrete is determined by air void parameters such as the air content, air void spacing factor (the distance between air void centers) and so on [28–30]. A proper air-void system is generally required to ensure the desirable F–T resistance [28]. The closed, small and evenly distributed air voids could provide some space for the accommodation of ice and, hence, effectively ease the ice expansion, thus enhancing the F–T resistance of concrete [30]. However, so far, the effects of MgO with different reactivity and dosage values on the air void and frost resistance of concrete have rarely been studied.

From the review of the existing literature, it can be seen that there are some studies concerning the effects of MgO on the water permeability and F–T resistance of concrete. Nevertheless, there is still a lack of information regarding the influence of MgO with different dosages and reactivities on the air void parameters, pore structure, impermeability and F–T resistance of concrete. Therefore, this paper intends to remedy this inadequacy. First, the effects of MgO with different contents (0, 4 wt.% and 8 wt.%, by weight of the binder) and reactivities (50 and 300 s) on the water penetration as well as the resistance of concrete to 300 F–T cycles were systemically investigated and compared. Then, the parameters of the pores, ranging from nano- to micro- scales, including the capillary pores (2.5–10μm) and air voids (pore size exceeding 10 μm), were investigated via a mercury intrusion porosimeter (MIP) and a linear traverse method, respectively. Finally, considering the fractal theory is an innovative method to analyze the pore structure of concrete, which exhibits obvious fractal characteristics [31–34], the permeability and F–T resistance of

concrete were analyzed via pore structural and fractal analysis. The outcomes of this study may reveal how MgO affects the impermeability and F–T resistance of concrete from a new perspective and also help engineers to select the optimal MgO reactivity and dosage for the proper application of MgO in practice.

2. Materials and Analytical Methods

2.1. Raw Materials

In this study, P·I Portland cement with a 28-day strength of 48.6 MPa and a MgO expansive agent with two reactivities, namely 50 s and 300 s, were used. The reactivity of MgO, which is the time needed for 1.7 g MgO to neutralize 200 mL of citric acid with a molar concentration of 0.07 mol/L, was tested according to the standards [35,36]. The two MgO, which are labelled M50 and M300, meet the standard requirements for reactive MgO (with a neutralization time between 50 and 200 s) and weak reactive MgO (with a neutralization time ranging from 200 to 300 s), respectively, based on DL/T 5296-2013 [35]. The main physical properties and chemical compositions of cement and MgO are listed in Table 1.

Table 1. Physical properties and chemical compositions of P·I cement and MgO.

Parameters	P·I Cement	M50	M300
Chemicals (wt.%)			
CaO	61.3	2.4	2.6
SiO_2	19.3	1.3	1.4
Fe_2O_3	4.3	0.6	0.5
MgO	3.7	91.2	91.0
SO_3	2.6	0.1	0.1
Al_2O_3	4.7	0.1	0.1
Loss on ignition	1.2	3.7	3.1
Physical properties			
Blaine specific surface area (m^2/kg)	326	-	-
BET specific surface area (m^2/g)	0.91	31.2	12.50
Median particle size (D50, μm)	17.3	11.8	19.8
Specific gravity	3.20	3.51	3.50

Coarse aggregate with a particle size of 5–40 mm and fine aggregate with a maximal particle size of 5 mm sourced from crushed limestone was adopted in this work. The density for both coarse and fine aggregates is 2650 kg/m^3. The fineness modulus of fine aggregate is 2.71. The aggregates were kept at a saturated surface dry (SSD) condition before preparing concrete mixtures.

2.2. Mix Proportion Design

To investigate the effects of MgO with different dosages and reactivity on the mechanical properties, F–T resistance and water permeability of concrete, concrete with a C30 strength grade was prepared. The concrete mixture proportion was designed based on the volume method according to Chinese standard DL/T 5330 (Code for mix design of hydraulic concrete) [37] and Ref. [38]. The MgO replacement for cement ratios of 0, 4 wt.% and 8 wt.% were adopted to prepare concrete. The polycarboxylate-based superplasticizer at a dosage of 0.6–0.9% (by weight of binder) and an air-entraining agent (AEA) at a dosage of 0.025–0.045% (by weight of binder) were used to generate a target slump of approximately 50–70 mm and a target air content of approximately 5% in each fresh concrete mixture. The water-to-binder (W/B) ratio was usually adopted to produce conventional moderate-strength concrete, thus the W/B of 0.4 was used in this study. For all of the concrete mixtures, the water-to-binder (W/B) ratio, the sand volume ratio and the water content were kept constant at 0.4, 32% and 122 kg/m^3, respectively. The details of the mix proportions and the corresponding designations are exhibited in Table 2. For instance, the concrete containing 0 MgO, which is designated as "C0", serves as the control sample and

the concrete with M50 and M300 added at a dosage of 4 wt.% is denoted as "C4M50" and "C8M300", respectively. The concrete specimens were cured in a standard curing room (20 ± 2 °C and RH > 95%) until being tested.

Table 2. Mix proportions and notations of concrete.

Designations	W/B Ratio	MgO Dosage (wt.%)	Mix Proportions (kg/m^3)						Slump (mm)
			Water	Cement	MgO	Sand	Coarse Aggregate	Super Plasticizer	
C0	0.4	0	122	305	0	630	1339	1.8	65
C4M50	0.4	4	122	293	12	631	1340	2.4	55
C8M50	0.4	8	122	281	24	631	1341	2.7	51
C4M300	0.4	4	122	293	12	631	1340	2.1	62
C8M300	0.4	8	122	281	24	631	1340	2.4	57

2.3. Test Methods

2.3.1. Compressive Strength of Concrete

Compressive strength is one of the most basic mechanical properties of concrete. The compressive strengths of concrete were tested at 3, 28, 90 and 180 days complying with DL/T 5150 (test code for hydraulic concrete) [39] by means of an electronic universal testing machine with a capacity of 300 kN. The hydration ages of 3, 28 and 180 days denote the early age, middle age and long-term age of concrete, respectively, which are also the typical hydration ages to determine the properties of concrete according to DL/T 5150. The concrete cubic specimens sized 150 mm × 150 mm × 150 mm were tested at a constant loading rate of 0.3–0.5 kN/s. For each compressive strength result, six cubic specimens were used, and an average value was reported as the final result.

2.3.2. Water Impermeability

Concrete impermeability refers to the ability to prevent external ions and water from entering the concrete, which is a dominant property affecting the durability of concrete, whereby the better the impermeability, the better the resistance to water and detrimental ion penetration [40,41]. The water impermeability test was conducted using a Hp–4.0 model permeability instrument, conforming to the procedure specified in DL/T 5150. Considering the concrete will not be subject to the water pressure in practical application at the very early hydration age, the 3-day permeability results of concrete were not tested in this work. During the test, six specimens cured for 28 and 180 days with a top diameter, bottom diameter and height of 185 mm, 150 mm and 175 mm, respectively, were tested for each concrete mixture. The test procedure is as follows: Before the test, the round surfaces of the cylindrical specimens were coated with a layer of hot wax to prevent leakages during the tests, then the specimens were placed in the instrument. Both the top surface and bottom surface of the cylinders were exposed so that the water can permeate through the concrete under high water pressure. Once the sealing procedure was completed, water was injected into the bottom space of the specimens and the water pressure was increased directly to 1.4 MPa and maintained for 24 h, then the water pressure was unloaded, and the specimens were split into two parts. After that, the average water-seepage height (D_m) of each group of concrete specimens was calculated. Based on the D_m values, the relative permeability coefficient (K_r) of concrete can be calculated by the following Equation (1):

$$K_r = aD_m^2/2TH \quad (1)$$

where K_r is the relative permeability coefficient, cm/h; T is the duration of the test, which is 24 h; H is the water head, which is 12,244 cm in this work; a is the absorption ratio of concrete, which is 0.03.

2.3.3. Freezing and Thawing (T–F) Resistance Test

The frost resistance of concrete was tested based on the method of rapid freezing and thawing in water conforming to DL/T 5150 [39]. This test procedure is nearly the same as Method A specified in ASTM C666 [42]. During the T–F resistance test, three specimens (400 mm × 100 mm × 100 mm) cured for 28 and 180 days of each concrete mix were used to measure the frost resistance, and the average test results were reported. For each test, the concrete specimens were subjected to 300 T–F cycles. Before the test, the initial mass and transverse frequency of each specimen were recorded first, and then the T–F tests were conducted at a rate of 6 cycles per day. Each T–F cycle comprises a rapid temperature drop period (maintained at −17 °C) of 2.5 h and a rapid temperature rise period (from −17 °C to 8 °C) of 1.5 h. The freezing and rising rate in the test is approximately 4 °C/h. The mass loss and transverse frequencies were tested and recorded every 50 cycles up to 300 cycles. Similarly, concrete at an early age is commonly well cured in practice and therefore will not suffer from F–T resistance at a very early curing age, hence the 3-day F–T resistance tests were not conducted.

2.3.4. Pore Structure Evaluation by Mercury Intrusion Porosimeter (MIP)

In this study, the porosity and pore size distribution of concrete cured for 3, 28 and 180 days were measured by MIP using Micromeritics AutoPore IV 9500 (U.S.A.) with a pressure range of 0–414 MPa, which could test the pore size with a range of approximately ~2 nm to 10 μm. MIP samples were obtained by cutting small cubic pieces sized approximately 5–8 mm from the center of concrete specimens for strength tests using a diamond saw. The coarse aggregates were moved from the MIP samples before the MIP tests, which can be easily accomplished since the coarse aggregates are grey and can be distinguished by the naked eye. Before the test, the cubic pieces were immersed in ethanol for 24 h to remove the free water, and then dried at 60 °C for 5 h to a constant mass in a vacuum drying oven. At least three samples were placed into the glass tube for each MIP test to minimize the effects of variations in sample size on test results.

2.3.5. Air Void Evaluation by The Linear Traverse Method

A proper air-void system plays a key role in maintaining good F–T resistance of concrete. The air void structure parameters of concrete cured for 3, 28 and 180 days, including the air void spacing, air void number and size, were evaluated using a Rapidair 457 air void analyzer, conforming to the linear traverse method described in detail in ASTM C 457 [43]. This air void analyzer could test air voids with sizes ranging from approximately 10 μm to 2000 μm. A picture of this analyzer device and the testing procedure of the air-void system were presented in detail in our previous studies [21,34]. The concrete samples with a size of 150 mm × 150 mm × 150 mm were cured for 3, 28 and 180 days in a foggy room with a temperature of 20 ± 2 °C and relative humidity of 95 ± 2% before the air void test. The tested concretes were sawed into slices with a size of 1 cm × 15 cm × 15 cm, then the concrete slices were used for the air void test. During the test, the surfaces of slices were polished until smooth and painted with a layer of fluorescent powder. The air voids filled with fluorescent powder can be detected by ultraviolet irradiation from the analyzer. For each slice, seven linear traverses were evenly arranged on the slice surface, thus the total length of linear traverses for each slice was 1050 mm. For each concrete mix, three slices made from different concrete specimens were tested, and the average air void result was reported.

2.3.6. Calculation of Fractal Dimension

Pfeifer and Avnir [44] demonstrated that the roughness and irregularities of pore surfaces of porous material can be characterized by the fractal dimension of pore surface fractal dimension (D_s). In this work, Zhang's fractal model [45,46], based on MIP results, was employed to obtain the D_s of concrete.

According to Zhang's model [45,46], there is a logarithmic correlation between the accumulated injection work (W_n) on mercury and the total volume mercury injected into the pores (V_n), as shown in Equation (2):

$$ln\frac{W_n}{r_n^2} = \mathrm{D_s} ln\frac{V_n^{1/3}}{r_n} + C \quad (2)$$

where r_n is the pore radius m; C is a regression constant; n represents the n-th mercury injection.

W_n can be calculated by the following Equation (3):

$$W_n = \sum_i^n p_i \triangle V_i \quad (3)$$

where the index i is the i-th mercury injection; p_i refers to as the mercury pressure Pa; V_i denotes the volume of mercury injected at the i-th injection, m^3.

The values of W_n, V_n, $ln\frac{W_n}{r_n^2}$ and $ln\frac{V_n^{1/3}}{r_n}$ can be calculated directly from the MIP results and Equation (3). Then $\mathrm{D_s}$ can be determined, which is the slope of the straight line in Equation (2).

3. Results and Discussion

3.1. Compressive Strength of Concrete

The compressive strength of concrete containing MgO with different reactivity and content at 3, 28, 90 and 180 days is exhibited in Figure 1. The error bars of the mechanical property results are also shown in Figure 1.

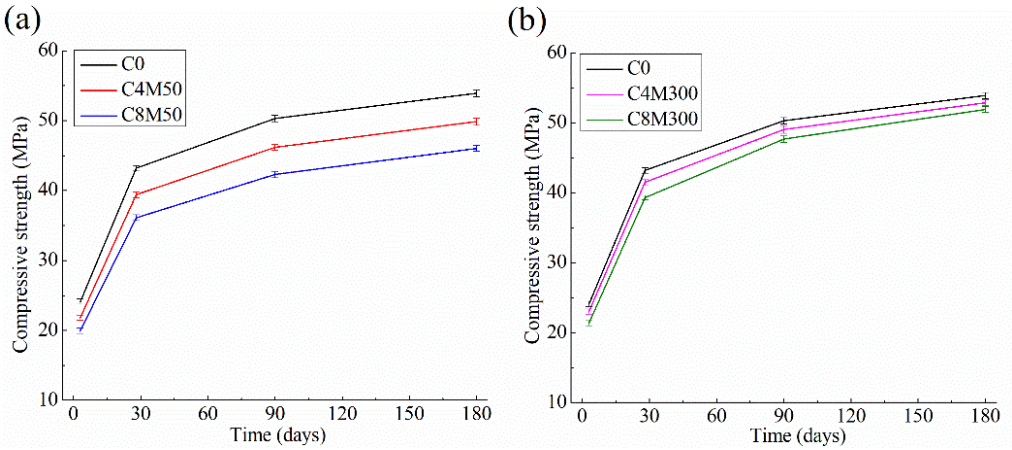

Figure 1. Compressive strength of concrete containing MgO with reactivity of (**a**) 50 s and (**b**) 300 s.

Figure 1 indicates both M50 and M300 could reduce the compressive strength of concrete, and at a higher dosage of MgO, a larger reduction in compressive strength can be observed. The reduced compressive strength of concrete in the presence of MgO can be attributed to several reasons: (1) The dilution effect due to MgO addition leads to a reduced cement amount, which inevitably leads to the generation of less hydration product and weakens the concrete strength to some degree [47,48]. (2) The reaction product of MgO with water is brucite crystal, which is not helpful for, or even weakens, the strength gain of concrete since brucite cannot act as a binding phase like calcium silicate hydrate (C-S-H) [49–53]. (3) Some studies reported that the consumption of water by MgO, as well as the generation of micro-cracks and high porosity accompanied by brucite expansion, should be held responsible for the weakened concrete strength [1,47,48]. The higher dosage of MgO would result in a stronger dilution effect, while it could also consume more of the water mixture and produce more brucite crystals, thus leading to a larger strength reduction.

However, a comparison of the results in Figure 2 shows that concrete with different reactivities of MgO exhibits different strength development; that is, at the same dosage level, the incorporation of reactive M50 decreases the compressive strength of concrete more significantly than M300, especially at an early age. Specifically, the addition of 8 wt.% M50 lowers the compressive strength of C0 by about 17.2%, 16.4%, 15.9% and 14.6% at 3, 28, 90 and 180 days, while the reductions are only 11.3%, 9.0%, 5.2% and 3.7%, respectively, due to the addition of 8 wt.% M300. The same phenomenon can be found for concrete containing 4 wt.% MgO with different reactivity in a similar study [50]. Cao et al. [50] concluded that the addition of reactive MgO in concrete would produce much weaker mechanical properties at an early age. An experimental study concerning the MgO reaction [54] indicates that the reaction degree of 325 s MgO is less than 10% while that of 46 s MgO is nearly 100%, revealing most highly reactive MgO can act with water at an early age, whereas weakly reactive MgO rarely reacts with water at the initial time. These quantitative results could reasonably support the observed difference in strength reductions described above, i.e., M50 reacts with water quickly, consuming more free water and producing more brucite crystals than M300, which inevitably results in larger strength reductions.

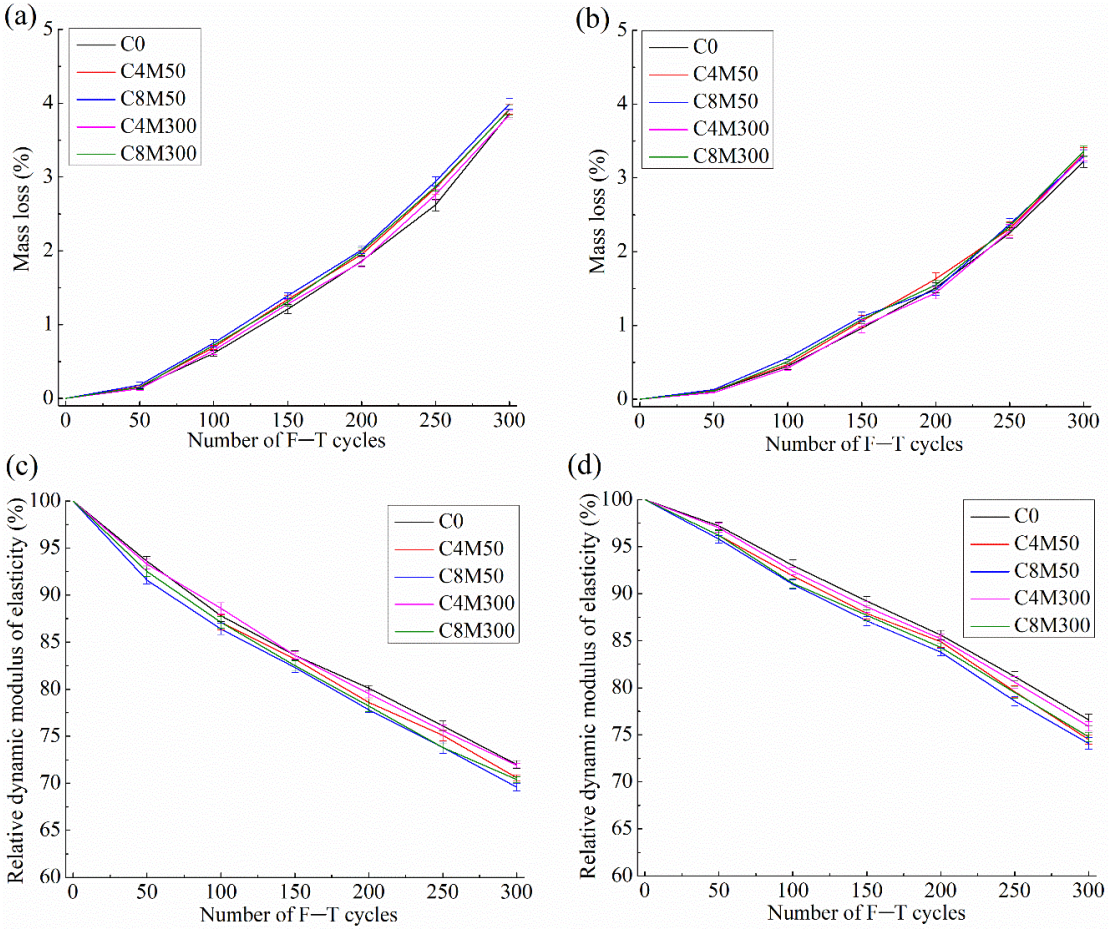

Figure 2. F–T resistance results of concrete; (**a**) 28-day mass loss, (**b**) 180-day mass loss, (**c**) 28-day relative dynamic elastic modulus and (**d**) 180-day relative dynamic elastic modulus.

In addition, it can be seen from Figure 2 that the presence of M300 could contribute to the long-term strength increase, while M50 could not. For example, the 180-day strength gap between C8M300 and C0 is only 3.7%, while the gap between C8M50 and C0 is as large as 14.6% at 180 days. This trend is in good agreement with the findings in another study [25], which reported that concrete containing 5% MgO with a weak reactivity of 265 s

starts to increase in compressive strength after 56 days of curing and reaches almost the same 180-day strength as plain concrete. A similar trend can be observed from cement mortars by Cao et al. [50]. These researchers ascribed this trend to the fact that MgO with weak reactivity begins to react with water at the middle hydration age and thereafter it could densify the pore structures, hence lowering the strength gap between MgO concrete and the control concrete at a later age. In contrast, due to its high reaction degree at an early age, reactive MgO could not improve the pore structure and facilitate the long-term strength of concrete, as evidenced by the study [54]. This statement will be supported by MIP results in Section 3.4.

3.2. Permeability

The permeability results of concrete including the water-seepage height (D_m) and relative permeability coefficient (K_r) at 28 and 180 days are shown in Table 3. Table 3 shows the reactivity and dosage of MgO obviously affect the permeability of concrete.

Table 3. The 28-day and 180-day permeability of concretes containing MgO with different reactivity and dosage.

Designations	Curing Time (Days)	Average Water Seepage Height D_m (cm)	Relative Permeability Coefficient K_r ($\times 10^{-7}$ cm/h)
C0	28	3.5 ± 0.12	6.25 ± 0.43
	180	2.7± 0.14	3.72 ± 0.39
C4M50	28	3.1 ± 0.1	4.91 ± 0.32
	180	2.2 ± 0.11	2.47 ± 0.25
C8M50	28	2.7 ± 0.14	3.72± 0.39
	180	1.8 ± 0.12	1.65 ± 0.22
C4M300	28	3.5 ± 0.13	6.25 ± 0.47
	180	1.9 ± 0.12	1.84 ± 0.23
C8M300	28	3.6 ± 0.10	6.62 ± 0.37
	180	1.4 ± 0.11	1.00 ± 0.16

Table 3 shows the inclusion of reactive M50 improves the impermeability of concrete at 28 days. Specifically, the 4 wt.% addition of M50 lowers the D_m and K_r values of C0 concrete by about 11.4% and 21.5% at 28 days, respectively, and the increase in M50 dosage from 4 wt.% to 8 wt.% further reduces the D_m and K_r values by about 23.0% and 40.5%, respectively, compared with C0. On the contrary, the D_m and K_r values of concrete cured for 28 days did not change with the addition of weak-reactivity M300. Nevertheless, it is clear from Table 3 that the presence of 4 wt.% M300 considerably lowers the D_m and K_r values of concrete at 180 days by about 45.7% and 70.5%, respectively, compared with C0 concrete. Moreover, the higher dosage of M300 would enhance this beneficial effect to a larger extent. The results above demonstrate that M50 is beneficial for the improvement in impermeability of concrete at an early age while M300 is beneficial for impermeability at a long-term age. It is well accepted that the impermeability of concrete depends on the pore structure of concrete. As revealed by Zheng et al. [24], the permeability was governed by the volume fraction (total porosity) and microgeometry of the entire pore structure in concrete. In this study, the enhanced resistance to water permeability may also be associated with the variations in pore structure due to MgO addition. This presumption will be verified from the standpoint of pore structure in Section 3.4.2.

3.3. F–T Resistance

The results of the F–T resistance of concrete containing MgO with different reactivity and dosage at 28 and 180 days are exhibited in Figure 2. Figure 2 shows the reactivity and dosage of MgO obviously affect the F–T resistance of concrete.

According to DL/T 5150 [39] and ASTM C666 [42], the mass loss and the relative dynamic elastic modulus are two typical results of the F–T resistance test to assess the

F–T resistance of concrete. There are two important criteria to evaluate whether concrete achieves F–T resistance of F(n), that is, the mass loss of the concrete specimen is less than 5% and the relative dynamic modulus of elasticity is decreased less than 40% after n F–T cycles. From Figure 2, it can be seen that all of the concretes in this work exhibit mass losses less than 5% and relative dynamic modulus of elasticity larger than 60% after 300 T–F cycles, indicating all of the concretes have an F–T resistance grade of F300 according to DL/T 5150 [39].

As shown in Figure 2, during all 300 F–T cycles, the differences among all concrete containing MgO with different reactivity and content are minor at the same hydration age. What is more, these differences seem to fall within the error range, indicating the influence of MgO on F–T resistance can be seen as negligible in this study. This finding agrees well with the study by Choi et al. [25], who found MgO might have little effect on the F–T resistance of concrete because MgO would not change the pores larger than 10 μm within MgO concrete. The F–T resistance of concrete will be further discussed in terms of air void parameters in Section 3.5.

3.4. Pore Structures and Pore Structural Analysis of Durability

3.4.1. Pore Structures

The pore structure parameters of concrete containing MgO with different reactivities and dosage at 3, 28 and 180 days are exhibited in Table 4. On the basis on the classical method [55], pores with the size ranges of 2.5–10 nm, 10–50 nm, and 50 nm–10 μm can be divided into small capillary pores (also called gel pores), medium capillary pores and large capillary pores, respectively. Table 4 indicates MgO reactivity and dosage have an important impact on concrete pore structure [23].

Table 4. Pore structure parameters of concrete obtained by MIP.

Designations	Hydration Age (Days)	The Most Probable Pore Diameter (nm)	Porosity (%)	Pore Size Distribution		
				<10 nm (%)	10–50 nm (%)	50 nm–10 μm (%)
C0	3	166.0	33.6	7.2	23.9	68.6
	28	73.3	23.6	13.2	42.6	43.6
	180	41.6	19.8	20.6	53.2	25.9
C4M50	3	151.3	29.6	7.1	31.2	61.1
	28	63.5	20.3	12.9	46.9	40.1
	180	35.5	17.7	20.9	58.9	19.4
C8M50	3	126.4	25.5	6.8	38.9	54.2
	28	52.3	17.3	13.0	52.1	34.6
	180	26.9	14.5	19.7	64.8	14.9
C4M300	3	168.2	34.2	7.1	22.9	69.5
	28	74.6	24.3	12.9	41.4	45.2
	180	29.6	14.7	19.6	63.8	15.9
C8M300	3	170.6	33.1	6.8	22.8	69.5
	28	72.9	24.2	12.5	51.9	35.4
	180	21.3	11.8	20.9	68.1	10.8

As illustrated in Table 4, the addition of M50 can refine the pores in concrete at 3 and 28 days, whereas the weak-reactivity M300 cannot. For instance, for the proportion of large capillary pores (between 50 nm and 10 μm), the porosity, as well as the most probable pore diameter, of concrete were obviously reduced in the presence of M50 at 3 and 28 days. The porosity of concrete was reduced from 33.6% to 29.6% and 25.5% due to the addition of M50 at the dosages of 4 wt.% and 8 wt.%, respectively. By contrast, these pore structure parameters do not vary with the addition of M300. These findings are in good agreement with those reported by Mo et al. [56], who conducted an MIP study on cement pastes and found the addition of 8 wt.% MgO with a high reactivity of 45 s lowers the porosity of control cement pastes and the addition of 8 wt.% weak reactive MgO (135 s)

does not change the pore structure parameters of pastes. Two possible reasons may be responsible for this trend. One reason is that the reactive MgO could quickly react with water to generate a large number of $Mg(OH)_2$ crystals to fill the pores at the initial hydration time, thus reducing the porosity and the fraction of large pores. However, weak-reactivity MgO cannot participate in the reaction with water so it cannot change the pore structure. This is well evidenced by quantitative analysis by Mo et al. [16], in which the amount of $Mg(OH)_2$ formed in cement pastes containing reactive MgO (65 s) at an early hydration age (e.g., within 28 days) was much higher than that in the pastes with weak-reactivity MgO added (145 s). The other possible reason is that the expansion of the $Mg(OH)_2$ crystals formed could cause refinement and densification in the pore structure of cement pastes and concrete [16,23].

Table 4 also shows that at 180 days, M300 exhibits a much stronger pore refinement effect than M50. In other words, the concrete with M300 added has a lower porosity, a smaller most-probable pore diameter and a lower proportion of large capillary pores than C0 and that with M50 added. For example, C4M300 cured at 180 days has a porosity of 14.7%, a most-probable pore diameter of 29.6 nm and a proportion of large capillary pores of 15.9%, all of which are smaller than those of C4M50 (17.7%, 35.5 nm and 19.4%, respectively). The same trend can be observed for cement mortars by Choi et al. [25], in which the porosity and proportion of large pores of mortars containing 5 wt.% weak reactive MgO (265 s) were obviously reduced compared with those of plain cement mortar at 360 days. This phenomenon can be attributed to the continuous reaction of weak reactive MgO at a late age, which could produce $Mg(OH)_2$ and refine the pore structures [25].

From Table 4, it is easy to observe the trend whereby a high dosage of MgO will produce a fine pore structure in concrete. For instance, the porosity, the most-probable pore diameter and the proportion of large capillary pores of C4M300 cured at 180 days are smaller than those of C8M300 at the same hydration age. The same trend can be observed for concrete containing M50 at 3 and 28 days. However, a contrary conclusion was reported by Cao et al. [1], who found the porosity and pore diameter of cement pastes containing 10 wt.% weak-reactivity MgO (220 s) are larger than those of pastes containing 6 wt.% MgO with the same reactivity. These seemingly reverse trends can be explained by the difference in MgO dosage in this work and in Cao et al.'s study [1]. In Cao et al.'s study [1], the scanning electron microscope (SEM) micrographs revealed that an excessive dosage (e.g., 10 wt.% or more) of MgO would generate a large amount of $Mg(OH)_2$ hexagonal lamellar crystals, and the growth of these crystals could increase the pore diameter, produce many additional pores and even micro cracks, leading to a harmful volume expansion of concrete. It is also interesting to note from Table 4 that the addition of both M50 and M300 could not reduce the fractions of small capillary (gel) pores. The mechanism behind this could be that the gel pore fraction is more related to the main cement hydration products, i.e., C-S-H and other gel phases [38], while the reaction product of MgO is $Mg(OH)_2$ crystals, which would not increase the amount of gel.

3.4.2. Pore Structural Analysis of Permeability and F–T resistance

The relationship between the permeability result of concrete and main pore structure parameters such as porosity and the fraction of large capillary pores (pore size between 50 nm and 10 μm) at 28 and 180 days are shown in Figure 3.

Figure 3 displays that K_r is linearly related to the porosity and fraction of large capillary pores. Some studies [24,41] have reported similar results that high porosity and a high proportion of large capillary pores favor the generation of seepage channels for water permeation and ion diffusion. Metha and Monterio [57] further demonstrated that pores with a size ranging from 50 nm to 0.1 μm significantly contribute to the permeability of concrete. Therefore, the permeability difference caused by MgO reactivity and dosage can be understood from the viewpoint of pore structure. As discussed in Section 3.4.1, reactive M50 can densify the pore structure of concrete and lower the fraction of large capillary pores at 28 days, so it can cut off the water and ion penetration channels as well

as improve the resistance of concrete to permeability at an early hydration age. In contrast, weakly reactive M300 can participate in the reaction with water and densify the pores of concrete at 180 days; consequently, the impermeability of concrete at a long-term age can be enhanced by M300. Considering hydraulic concrete only suffers from high water pressure at a long-term age, weakly reactive MgO at relatively high dosage is suggested for use in practical applications.

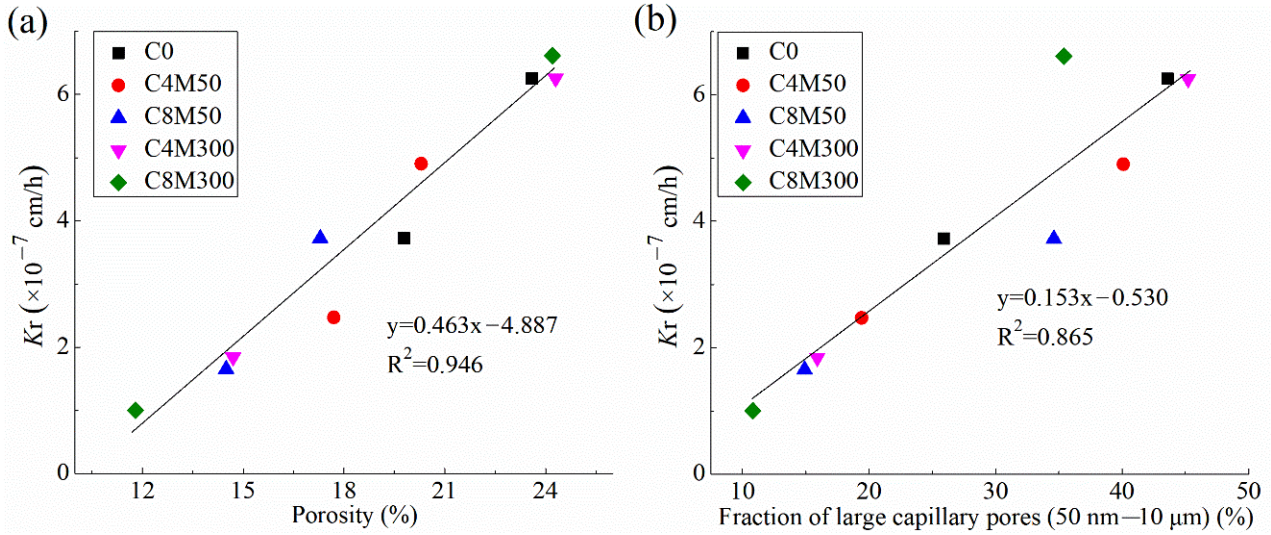

Figure 3. The correlations of relative permeability coefficient K_r with (**a**) fraction of pores sized between 50 nm and 10 μm (large capillary pores) and (**b**) porosity.

Moreover, a careful pore structural analysis of the F–T resistance found there are no definite correlations among the F–T resistance (e.g., mass losses and relative dynamic modulus of elasticity) and pore structural parameters (e.g., the porosity and the fraction of large capillary pores) of concrete. For instance, C0 concrete with the largest porosity and fraction of large capillary pores among all the concretes at 28 days does not exhibit the best or weakest F–T resistance, and this is also observed for C8M300, which has the smallest porosity and fraction of large capillary pores among all the concretes at 180 days. This is because the pore structures detected by MIP are not closely related to the F–T resistance of concrete [28]. The total porosity is not a good indicator of frost durability, since very small capillary pores would not contribute to the increase in F–T resistance [28]. As demonstrated by Powers and Brownyard [58], the nucleation of ice crystals becomes more difficult as the pore size decreases. Many other researchers proved that the F–T resistance of concrete is significantly affected by pores with a diameter above 50 μm [59] or around 300 μm [60], all of which are within the pore size range of air voids.

3.5. Air Void Parameters and Analysis

3.5.1. Air Void Parameters

The air void parameters of concrete containing MgO with different reactivities and dosage hydrated at 28 and 180 days, including the hardened air content (A), the total number of air voids (N), the average air void diameter (D) and the spacing factor (L), are shown in Table 5. Since early-age concretes are rarely subjected to F–T damage, the air void parameters of concretes are tested at 28 and 180 days in this work. These air void parameters are usually considered the main factors affecting the F–T resistance of concrete [30]. For instance, adequate entrained air voids in concrete are needed to guarantee the desirable F–T resistance [28], since the entrained air voids can provide enough spare space to accommodate the ice expansion [40,58]. In addition, under the same air content in concrete, a smaller air void diameter and a greater number of air voids would result in a smaller air

void spacing factor $\bar{L}$ and, consequently, better F–T resistance [30]. Many studies confirmed that an $\bar{L}$ value below 250 μm is necessary for a desirable F–T resistance of concrete [28,30]. On the basis of this criterion, all of the $\bar{L}$ results in Table 5 below 250 μm indicate all of the concretes in this work possess good F–T resistance.

Table 5. Air void parameters of 28-day and 180-day concretes containing MgO with different reactivities and dosage.

Designations	Hydration Age (Days)	Total Number of Air Voids N	Traverse Length through Air Ta (mm)	Hardened Air Content A (%)	Average Chord Length l (μm)	Average Air Void Diameter (μm)	Spacing Factor $\bar{L}$ (μm)
C0	28	720	154	4.9	214	161	235
	180	710	151	4.8	213	160	233
C4M50	28	782	151	4.8	193	145	214
	180	759	154	4.9	203	153	225
C8M50	28	798	145	4.6	182	136	204
	180	755	142	4.5	188	141	211
C4M300	28	765	148	4.7	194	145	216
	180	741	145	4.6	196	147	218
C8M300	28	766	145	4.6	189	142	213
	180	735	148	4.7	201	151	227

It should be noted that the target air content of all of the fresh concrete was kept as 5%, and it can be seen from Table 5 that there is no appreciable difference in hardened air content (A). In addition, Table 5 clearly illustrates that MgO dosage and reactivity have almost no influence on the air void parameters of concretes. This result is similar to those in other studies [21]. Wang et al. [21] found the incorporation of 6 wt.% reactive MgO (65 s) has no refinement effect on air voids in concrete cured for 28 days. Similarly, Choi et al. [25] reported that there was no change in pores larger than 10 μm within concrete with weak reactive MgO (265 s) added, hydrated at the long-term age of 360 days. The MIP results in Section 3.4 revealed that the MgO addition could refine the large capillary pores (50 nm–10 μm) due to the expansion of $Mg(OH)_2$ crystals. Nevertheless, such an expansion may not be large enough to densify the air voids, the size of which are 15–20 times as large as those of large capillary pores, as shown in Table 5.

3.5.2. Air Void Analysis of Permeability and F–T resistance

As Table 3 indicates, MgO reactivity and dosage obviously affect the permeability of concrete, while they do not change the air void parameters. As a consequence, there are no definite correlations between the permeability property of concrete (K_r) and air void parameters.

In addition, it is clear from Figure 2 and Table 5 that the differences in F–T resistance and air void parameters among all of the concretes hydrated at the same age are minor, that is to say, MgO addition within the dosage and reactivity range in this work would not change the F–T resistance or air void parameters. Based on the above discussion, a trend between the F–T resistance and air void parameters cannot be confirmed. Perhaps a higher dosage, e.g., 10 wt.% or more, would have a considerable influence, but this high dosage is of no practical use since it is beyond the maximum dosage for practical application.

3.6. Fractal Dimension of Pore Surface (D_s) and Fractal Analysis

3.6.1. Fractal Dimension of Pore Surface (D_s)

D_s values of concretes containing MgO with different reactivity and dosage at 3, 28 and 180 days are shown in Table 6. Table 6 also shows the R^2 values of the fitting lines shown in Equation (2), which approach 1.0, indicating the calculated D_s values are of adequate accuracy and reliability.

Table 6. Fractal dimension of pore surface (D_s) of concretes added with MgO.

Designations	Hydration Age (Days)	D_s	R^2
C0	3	2.658	0.946
	28	2.835	0.974
	180	2.925	0.956
C4M50	3	2.765	0.965
	28	2.876	0.946
	180	2.941	0.957
C8M50	3	2.815	0.980
	28	2.912	0.957
	180	2.968	0.967
C4M300	3	2.651	0.978
	28	2.838	0.983
	180	2.972	0.984
C8M300	3	2.667	0.988
	28	2.836	0.991
	180	2.983	0.992

Based on the fractal theory, D_s values of porous material are meaningful between 2.0 and 3.0, and an object with a D_s value >3.0 or <2.0 is considered to be non–fractal [31,34,41,61]. Additionally, a D_s value close to 2 indicates the measured object has a smooth surface, while a D_s value approaching 3 means the pore structure becomes rougher and more complex [62]. Table 6 shows that all of the concretes have D_s values between 2.658 and 2.983. Therefore, the pore structures of concretes containing MgO with different reactivities and dosage in this work have obvious fractal characteristics.

Figure 4 reveals the close correlation between the pore structure of concrete and D_s. Specifically, D_s is negatively correlated with both the porosity and the most-probable pore diameter of concrete, with high R^2 values of 0.970 and 0.938, respectively, indicating D_s can aptly reflect the pore structures. As Jin et al. [63] reported, D_s can perform more accurately and sensitively than other pore structure parameters to characterize the overall pore structures.

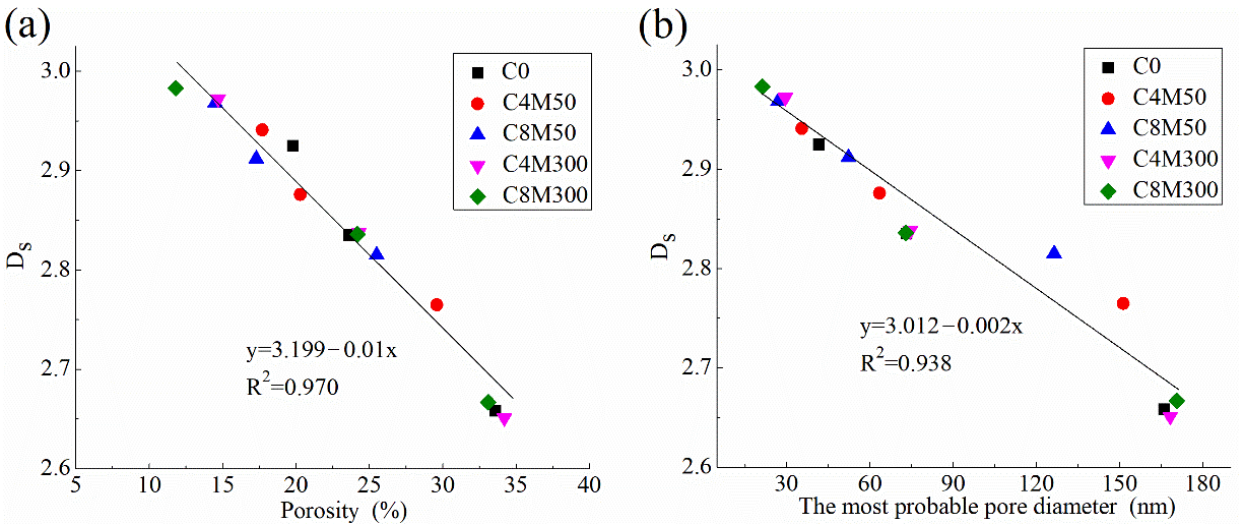

Figure 4. The correlation between D_s and (**a**) porosity and (**b**) the most-probable pore diameter of concrete.

3.6.2. Fractal Analysis of Permeability and F–T Resistance

The correlation between the permeability of concrete and D_s is exhibited in Figure 5.

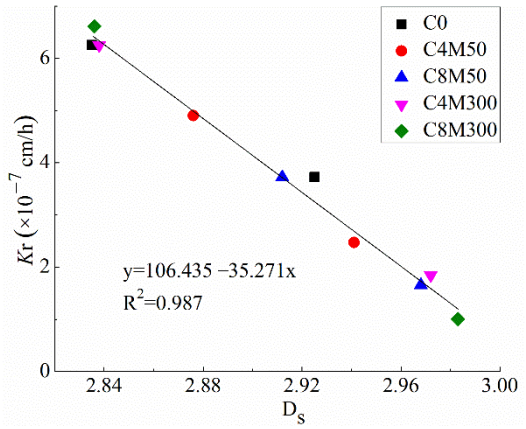

Figure 5. The correlation between the relative permeability coefficient (K_r) and D_s.

Figure 5 clearly shows K_r is negatively correlated with D_s, with a high R^2 value of 0.987. That is to say, the larger the value of D_s, the better the impermeability. A similar close relationship between the permeability of concrete and D_s has been reported in other studies [41] conducted on chloride permeability. Both of these studies confirmed that D_s could reflect the porosity and permeability of concrete. Accordingly, the difference in the effects of MgO on the permeability of concrete can by explained from the viewpoint of D_s. In specific, M50 can react with water at an early age and refine the pore structure, thus increasing the roughness and irregularities of pores and improving the impermeability of concrete. On the contrary, M300 begins to densify the pore structures at a later age and produces the smallest porosity and the most irregular pore structures among all of the concretes, resulting in the largest D_s and greatest impermeability of concrete.

The relationship between the F–T resistance of concrete and D_s is revealed in Figure 6. Figure 6 shows that there are no correlations between the F–T resistance of concrete and D_s, since the data are so scattered in Figure 6. This is because MgO in this work significantly affects the pore structures and the corresponding D_s, while it cannot affect the F–T resistance of concrete. As discussed above, the F–T resistance of concrete is affected by air voids rather than by the capillary pores detected by MIP. Based on the discussion above, it can be concluded that D_s is not suitable to analyze the F–T resistance.

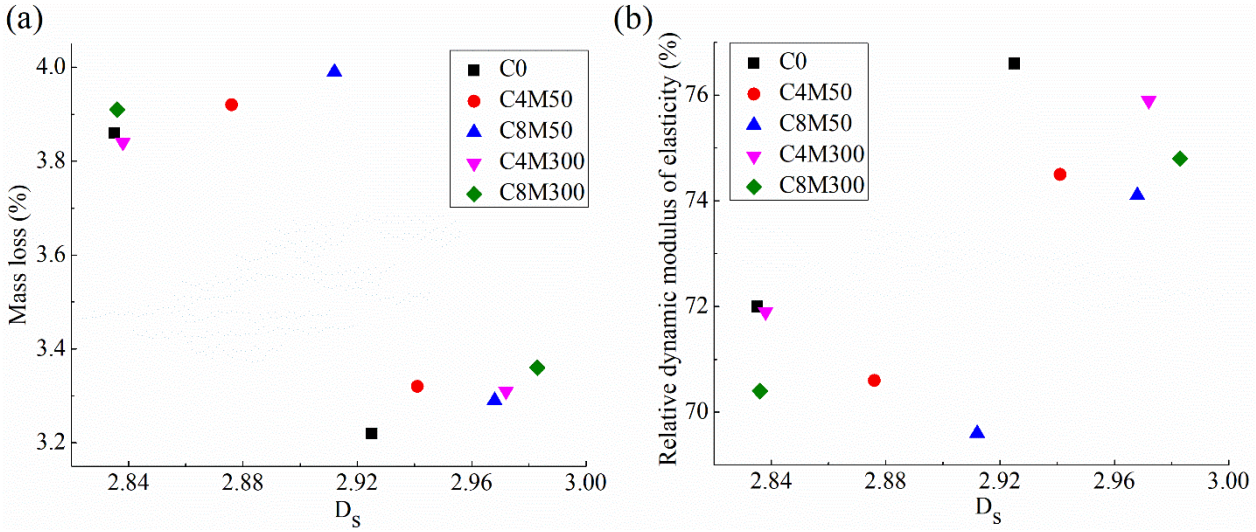

Figure 6. The correlation between D_s and (**a**) mass loss and (**b**) relative dynamic elastic modulus of concrete.

4. Conclusions

The following conclusions can be obtained:

(1) The addition of 4–8 wt.% reactive MgO (M50) and weakly reactive MgO (M300) lowers the compressive strength of concrete by 4.4–17.2%, 3.9–16.4% and 1.9–14.6% at 3, 28 and 180 days, respectively. The increase in MgO dosage and reactivity tends to further reduce the concrete strength at all hydration ages. The presence of M300 contributes to the long-term strength increment, while M50 cannot.

(2) Permeability of concrete is linearly related to the porosity and fraction of large capillary pores. M50 can densify the pore structure and lower the fraction of large capillary pores at an early age, thus it is beneficial for the impermeability of concrete at an early age. In contrast, weakly reactive M300 can enhance the impermeability of concrete at 180 days since it can densify the pore structure of concrete, but only at a later age. The weakly reactive M300, at a relatively high dosage of 8 wt.%, is suggested to be used in hydraulic concrete.

(3) The influence of MgO on F–T resistance is minor, since MgO could not change the air void parameters. Perhaps a higher dosage, e.g., 10 wt.% or more, would have a considerable influence, but this high dosage is beyond the maximum dosage for practical application.

(4) MgO concretes exhibit obvious fractal characteristics. The fractal dimension of the pore surface (D_s) exhibits a close relationship with the permeability property of concrete, thus the difference in the effects of MgO with different reactivity on permeability can be explained in terms of D_s. However, there is no correlation between F–T resistance and D_s.

More micro-structural investigations such as X-ray diffraction, nuclear magnetic resonance (NMR), SEM/energy dispersive X-ray (EDX), X-ray computed tomography (X-ray CT), etc., are needed to study the effects of MgO on the microstructure of concrete, as well as more types of fractal dimensions, e.g., the fractal dimension of pore volume and fractal dimension of pore tortuosity, etc., can be used to characterize the structure of concrete, which will be conducted in the near future.

Author Contributions: Conceptualization, writing—original draft, writing—review and editing, investigation, formal analysis, supervision, project administration funding acquisition, L.W. (Lei Wang, wanglei535250684@xauat.edu.cn); investigation, X.S., H.Y., L.W. (Lei Wang, 120100549@wut.edu.cn), S.T., B.W. and W.M. All authors have read and agreed to the published version of the manuscript.

Funding: The authors appreciate the financial support provided by the Opening Funds of the Belt and Road Special Foundation of the State Key Laboratory of Hydrology-Water Resources and Hydraulic Engineering (2020492311), Opening Funds of the State Key Laboratory of Building Safety and Built Environment and the National Engineering Research Center of Building Technology (BSBE2020-2), the Opening Project of the State Key Laboratory of Green Building Materials (2020GBM07) and the Natural Science Research Project of the Shaanxi Provincial Department of Education (20JK0722).

Institutional Review Board Statement: Studies not involving humans.

Informed Consent Statement: Studies not involving humans.

Data Availability Statement: The data that support the findings of this study are available from the corresponding author upon reasonable request.

Acknowledgments: The authors would like to thank all the anonymous referees for their constructive comments and suggestions.

Conflicts of Interest: The authors declare no conflict of interest.

References

1. Cao, F.; Miao, M.; Yan, P. Hydration characteristics and expansive mechanism of MgO expansive agents. *Constr. Build. Mater.* **2018**, *183*, 234–242. [CrossRef]
2. Wang, L.; Yang, H.; Dong, Y.; Chen, E.; Tang, S. Environmental evaluation, hydration, pore structure, volume deformation and abrasion resistance of low heat Portland (LHP) cement-based materials. *J. Clean. Prod.* **2018**, *203*, 540–558. [CrossRef]
3. Wang, X.; Yu, R.; Shui, Z.; Song, Q.; Zhang, Z. Mix design and characteristics evaluation of an eco-friendly ultra-high performance concrete incorporating recycled coral based materials. *J. Clean. Prod.* **2017**, *165*, 70–80. [CrossRef]

4. Yang, H.J.; Lee, H.; Hanif, A. Hydration characteristics and microstructure evolution of concrete with blended binders from LCD and OLED wastes. *Eur. J. Environ. Civ. Eng.* **2022**, 2032836. [CrossRef]
5. Xie, Z.; Zhu, Z.; Fu, Z.; Lv, X. Simulation of the temperature field for massive concrete structures using an interval finite element method. *Eng. Comput.* **2020**, *37*, 45. [CrossRef]
6. Wang, L.; Dong, Y.; Zhou, S.; Chen, E.; Tang, S. Energy saving benefit, mechanical performance, volume stabilities, hydration properties and products of low heat cement-based materials. *Energ. Build.* **2018**, *170*, 157–169. [CrossRef]
7. Zhang, P.; Wang, K.; Wang, J.; Guo, J.; Ling, Y. Macroscopic and microscopic analyses on mechanical performance of metakaolin/fly ash based geopolymer mortar. *J. Clean. Prod.* **2021**, *294*. [CrossRef]
8. Wang, L.; Yang, H.; Zhou, S.; Chen, E.; Tang, S. Mechanical properties, long-term hydration heat, shinkage behavior and crack resistance of dam concrete designed with low heat Portland (LHP) cement and fly ash. *Constr. Build. Mater.* **2018**, *187*, 1073–1091. [CrossRef]
9. Zhan, P.; He, Z. Application of shrinkage reducing admixture in concrete: A review. *Constr. Build. Mater.* **2019**, *201*, 676–690. [CrossRef]
10. Wang, X.; Wu, D.; Zhang, J.; Yu, R.; Hou, D.; Shui, Z. Design of sustainable ultra-high performance concrete: A review. *Constr. Build. Mater.* **2021**, *307*, 124643. [CrossRef]
11. Zhang, P.; Gao, Z.; Wang, J.; Wang, K. Numerical modeling of rebar-matrix bond behaviors of nano-SiO_2 and PVA fiber reinforced geopolymer composites. *Ceram. Int.* **2021**, *47*, 11727–11737. [CrossRef]
12. Zhang, P.; Wang, K.; Wang, J.; Guo, J.; Hu, S.; Ling, Y. Mechanical properties and prediction of fracture parameters of geopolymer/alkali-activated mortar modified with PVA fiber and nano-SiO_2. *Ceram. Int.* **2020**, *46*, 20027–20037. [CrossRef]
13. Wang, L.; Zhou, S.; Shi, Y.; Tang, S.; Chen, E. Effect of silica fume and PVA fiber on the abrasion resistance and volume stability of concrete. *Compos. Part B* **2017**, *130*, 28–37. [CrossRef]
14. Yuan, B.; Li, Z.; Zhao, Z.; Ni, H.; Su, Z.; Li, Z. Experimental study of displacement field of layered soils surrounding laterally loaded pile based on transparent soil. *J. Soil Sediment.* **2021**, *21*, 3072–3083. [CrossRef]
15. Yuan, B.; Li, Z.; Chen, Y.; Ni, H.; Zhao, Z.; Chen, W.; Zhao, J. Mechanical and microstructural properties of recycling granite residual soil reinforced with glass fiber and liquid-modified polyvinyl alcohol polymer. *Chemosphere* **2021**, *268*, 131652. [CrossRef] [PubMed]
16. Mo, L.; Fang, J.; Hou, W.; Ji, X. Synergetic effects of curing temperature and hydration reactivity of MgO expansive agents on their hydration and expansion behaviours in cement pastes. *Constr. Build. Mater.* **2019**, *207*, 206–217. [CrossRef]
17. Gao, P.; Wu, S.X.; Lin, P.H.; Wu, Z.R.; Tang, M.S. The characteristics of air void and frost resistance of RCC with fly ash and expansive agent. *Constr. Build. Mater.* **2006**, *20*, 586–590. [CrossRef]
18. Mo, L.; Deng, M.; Wang, A. Effects of MgO-based expansive additive on compensating the shrinkage of cement paste under non-wet curing conditions. *Cem. Conc. Compos.* **2012**, *34*, 377–383. [CrossRef]
19. Wang, L.; Li, G.; Li, X.; Guo, F.; Tang, S.; Lu, X.; Hanif, A. Influence of reactivity and dosage of MgO expansive agent on shrinkage and crack resistance of face slab concrete. *Cem. Conc. Compos.* **2022**, *126*, 104333. [CrossRef]
20. Cao, F.; Yan, P.Y. The influence of the hydration procedure of MgO expansive agent on the expansive behavior of shrinkage-compensating mortar. *Constr. Build. Mater.* **2019**, *202*, 162–168. [CrossRef]
21. Wang, L.; Guo, F.X.; Yang, H.M.; Wang, Y.; Tang, S.W. Comparison of fly ash, PVA fiber, MgO and shrinkage-reducing admixture on the frost resistance of face slab concrete via pore structural and fractal analysis. *Fractals* **2021**, *29*, 2140002. [CrossRef]
22. Cao, F.; Miao, M.; Yan, P.Y. Effects of reactivity of MgO expansive agent on its performance in cement-based materials and an improvement of the evaluating method of MEA reactivity. *Constr. Build. Mater.* **2018**, *187*, 257–266. [CrossRef]
23. Wang, L.; Lu, X.; Liu, L.; Xiao, J.; Zhang, G.; Guo, F.; Li, L. Influence of MgO on the hydration and shrinkage behavior of low heat Portland cement-based materials via pore structural and fractal analysis. *Fractal Fract.* **2022**, *6*, 40. [CrossRef]
24. Zheng, J.; Wong, H.S.; Buenfeld, N.R. Assessing the influence of ITZ on the steady-state chloride diffusivity of concrete using a numerical model. *Cem. Conc. Res.* **2009**, *39*, 805–813. [CrossRef]
25. Choi, S.; Jang, B.S.; Kim, J.H.; Lee, K.M. Durability characteristics of fly ash concrete containing lightly burnt MgO. *Constr. Build. Mater.* **2014**, *58*, 77–84. [CrossRef]
26. Jiang, F.; Deng, M.; Mo, L.W.; Wu, W.Q. Effects of MgO expansive agent and steel fiber on crack resistance of a bridge deck. *Materials* **2020**, *13*, 3074. [CrossRef]
27. Sherir, M.; Hossain, K.; Lachemi, M. Permeation and transport properties of self-healed cementitious composite produced with MgO expansive agent. *J. Mater. Civ. Eng.* **2018**, *30*, 2466. [CrossRef]
28. Şahmaran, M.; Özbay, E.; Yücel, H.; Lachemi, M.; Li, V. Frost resistance and microstructure of engineered cementitious composites: Influence of fly ash and micro polyvinyl alcohol fiber. *Cem. Conc. Compos.* **2012**, *34*, 156–165. [CrossRef]
29. Nam, J.; Kim, G.Y.; Lee, B.; Hasegawa, R.; Hama, Y. Frost resistance of polyvinyl alcohol fiber and polypropylene fiber reinforced cementitious composites under freeze thaw cycling. *Compos. Part B* **2016**, *90*, 241–250. [CrossRef]
30. Zhang, P.; Liu, G.G.; Pang, C.M. Influence of pore structures on the frost resistance of concrete. *Mag. Concr. Res.* **2017**, *69*, 271–279. [CrossRef]
31. Xiao, J.; Xu, Z.; Murong, Y.; Lei, B.; Chu, L.; Jiang, H.; Qu, W. Effect of chemical composition of fine aggregate on the frictional behavior of concrete–soil interface under sulfuric acid environment. *Fractal Fract.* **2022**, *6*, 22. [CrossRef]
32. An, Q.; Chen, X.; Wang, H.; Yang, H.; Yang, Y. Segmentation of concrete cracks by using fractal dimension and UHK-net. *Fractal Fract.* **2022**, *6*, 95. [CrossRef]

33. Huang, J.; Li, W.; Huang, D.; Chen, E. Fractal analysis on pore structure and hydration of magnesium oxysulfate cements by first principle, thermodynamic and microstructure-based methods. *Fractal Fract.* **2021**, *5*, 164. [CrossRef]
34. Wang, L.; Zeng, X.; Yang, H.; Lv, X. Investigation and application of fractal theory in cement-based materials: A review. *Fractal Fract.* **2021**, *5*, 247. [CrossRef]
35. *DL/T 5296-2013*; Technical Specification of Magnesium Oxide Expansive for Use in Hydraulic Concrete, China. China Electric Power Press: Beijing, China, 2014.
36. *CBMF 19-2017*; Magnesium Oxide Expansive Agent for Concrete. China Building Materials Industry Press: Beijing, China, 2017.
37. *DL/T 5330-2015*; Code for Mix Design of Hydraulic Concrete, China. China Electric Power Press: Beijing, China, 2016.
38. Wang, L.; Guo, F.X.; Lin, Y.Q.; Yang, H.M.; Tang, S.W. Comparison between the effects of phosphorous slag and fly ash on the C-S-H structure, long-term hydration heat and volume deformation of cement-based materials. *Constr. Build. Mater.* **2020**, *250*, 118807. [CrossRef]
39. *DL/T 5150-2017*; Test Code for Hydraulic Concrete, China. China Electric Power Press: Beijing, China, 2017.
40. Chen, Y.; Cen, G.P.; Cui, Y.H. Comparative study on the effect of synthetic fiber on the preparation and durability of airport pavement concrete. *Constr. Build. Mater.* **2018**, *184*, 34–44. [CrossRef]
41. Wang, L.; Luo, R.Y.; Zhang, W.; Jin, M.M.; Tang, S. Effects of fineness and content of phosphorus slag on cement hydration, permeability, pore structure and fractal dimension of concrete. *Fractals* **2021**, *29*, 2140004. [CrossRef]
42. *ASTM C666/666M-15*; Standard Test Method for Resistance of Concrete to Rapid Freezing and Thawing. ASTM International: West Conshohocken, PA, USA, 2015.
43. *ASTM C457/457M-16*; Standard Test Method for Microscopical Determination of Parameters of The Air-Void System in Hardened Concrete. ASTM International: West Conshohocken, PA, USA, 2016.
44. Pfeifer, P.; Avnir, D. Chemistry in noninteger dimensions between two and three. I. Fractal theory of heterogeneous surfaces. *J. Chem. Phys.* **1983**, *79*, 3558–3565. [CrossRef]
45. Zhang, B.; Li, S.F. Determination of the surface fractal dimension for porous media by mercury porosimetry. *Ind. Eng. Chem. Res.* **1995**, *34*, 1383–1386. [CrossRef]
46. Zhang, B.; Liu, W.; Liu, X. Scale-dependent nature of the surface fractal dimension for bi- and multi-disperse porous solids by mercury porosimetry. *Appl. Surf. Sci.* **2006**, *253*, 1349–1355. [CrossRef]
47. Beshr, S.; Mohaimen, I.M.A.; Azline, M.N.N.; Azizi, S.N.; Nabilah, A.B.; Aznieta, A.A. Feasibility assessment on self-healing ability of cementitious composites with MgO. *J. Build. Eng.* **2021**, *34*, 101914. [CrossRef]
48. Mo, L.; Liu, M.; Al-Tabbaa, A.; Deng, M. Deformation and mechanical properties of the expansive cements produced by inter-grinding cement clinker and MgOs with various reactivities. *Constr. Build. Mater.* **2015**, *80*, 1–8. [CrossRef]
49. Wang, L.; Jin, M.; Zhou, S.; Tang, S.W.; Lu, X. Investigation of microstructure of C-S-H and micro-mechanics of cement pastes under NH_4NO_3 dissolution by ^{29}Si MAS NMR and microhardness. *Measurement* **2021**, *185*, 110019. [CrossRef]
50. Cao, F.; Yan, P.Y. Effects of reactivity and dosage of magnesium oxide expansive agents on long-term volume variation of concrete. *J. Chin. Ceram. Soc.* **2018**, *46*, 1126–1132.
51. Wang, L.; He, Z.; Cai, X.H. Characterization of pozzolanic reaction and its effect on the C-S-H gel in fly ash-cement paste. *J. Wuhan Univ. Technol.* **2011**, *26*, 320–325. [CrossRef]
52. Tang, S.; Wang, Y.; Geng, Z.C.; Xu, X.F.; Yu, W.Z. Structure, fractality, mechanics and durability of calcium silicate hydrates. *Fractal Fract.* **2021**, *5*, 47. [CrossRef]
53. Wang, L.; Yang, H.Q.; Zhou, S.H.; Chen, E.; Tang, S.W. Hydration, mechanical property and C-S-H structure of early-strength low-heat cement-based materials. *Mater. Lett.* **2018**, *217*, 151–154. [CrossRef]
54. Mo, L.; Deng, M.; Tang, M.S. Effects of calcination condition on expansion property of MgO-type expansive agent used in cement-based materials. *Cem. Conc. Res.* **2010**, *40*, 437–446. [CrossRef]
55. Mindess, S.; Young, J.F.; Darwin, D. *Concrete*; Prentice-Hall: Murray Hill, Japan, 2003.
56. Mo, L.; Fang, J.W.; Huang, B.; Wang, A.G.; Deng, M. Combined effects of biochar and MgO expansive additive on the autogenous shrinkage, internal relative humidity and compressive strength of cement pastes. *Constr. Build. Mater.* **2019**, *229*, 116877. [CrossRef]
57. Metha, P.K.; Monterio, P.J.M. *Concrete: Structure, Properties and Materials*, 4th ed.; McGraw-Hill: New York, NY, USA, 2013.
58. Powers, T.; Brownyard, T.L. Studies of the physical properties of hardened Portland cement paste- Part 8. The freezing of water in hardened Portland cement paste. *J. Am. Concr. Inst.* **1947**, *18*, 933–969.
59. Neville, A.M. *Properties of Concrete*, 4th ed.; Longman: London, UK, 2000.
60. Shon, C.; Abdigaliyev, A.; Bagitova, S.; Chung, C.W.; Kim, D. Determination of air-void system and modified frost resistance number for freeze-thaw resistance evaluation of ternary blended concrete made of ordinary Portland cement/silica fume/class F fly ash. *Cold Reg. Sci. Technol.* **2018**, *155*, 127–136. [CrossRef]
61. Xiao, J.; Long, X.; Qu, W.; Li, L.; Jiang, H.; Zhong, Z. Influence of sulfuric acid corrosion on concrete stress-strain relationship under uniaxial compression. *Measurement* **2021**, *187*, 110318. [CrossRef]
62. Wang, L.; Jin, M.M.; Guo, F.X.; Wang, Y.; Tang, S.W. Pore structural and fractal analysis of the influence of fly ash and silica fume on the mechanical property and abrasion resistance of concrete. *Fractals* **2021**, *29*, 2140003. [CrossRef]
63. Jin, S.; Zhang, J.X.; Han, S. Fractal analysis of relation between strength and pore structure of hardened mortar. *Constr. Build. Mater.* **2017**, *135*, 1–7. [CrossRef]